Hindawi
Mathematical Problems in Engineering
Volume 2018, Article ID 2592613, 13 pages
https://doi.org/10.1155/2018/2592613

Research Article

A Finite Segment Method for Skewed Box Girder Analysis

Xingwei Xue, Jiawei Wu, Junlong Zhou, and Hongnan Li

School of Civil Engineering, Shenyang Jianzhu University, Shenyang 110168, China

Correspondence should be addressed to Junlong Zhou; 13889341820@163.com

Received 21 November 2017; Accepted 9 January 2018; Published 13 February 2018

Academic Editor: Roman Lewandowski

A finite segment method is presented to analyze the mechanical behavior of skewed box girders. By modeling the top and bottom plates of the segments with skew plate beam element under an inclined coordinate system and the webs with normal plate beam element, a spatial elastic displacement model for skewed box girder is constructed, which can satisfy the compatibility condition at the corners of the cross section for box girders. The formulation of the finite segment is developed based on the variational principle. The major advantage of the proposed approach, in comparison with the finite element method, is that it can simplify a three-dimensional structure into a one-dimensional structure for structural analysis, which results in significant saving in computational times. At last, the accuracy and efficiency of the proposed finite segment method are verified by a model test.

1. Introduction

The continued economic development and increasing investment in infrastructure in China has resulted in a marked improvement in construction standards for transportation networks throughout the country. This investment and development include the increased design and implementation of high-speed rail lines, especially in the more populous eastern portion of the country [1]. Skew bridges are commonly used on high-speed railway lines due to their following advantages: (a) maintaining harmony with the surrounding buildings and environment by requiring less land space for the new structure; (b) reducing resistance to flow for piers located in the water; and (c) meeting high-speed rail performance demands. Compared with a bridge having an orthogonal substructure, the behavior of skewed bridges is more complicated due to torsional effects that result from the skew angle [2].

During the past few decades, experimental and computational studies of skewed highway bridges have been performed [3–6]. Scordelis et al. [7] presented the theoretical and experimental results of a 45° skew two-span four-cell reinforced concrete box girder bridge model with a 1 : 2.82 scale. Results are given for reactions, deflections, strains, and moments due to working stress point loads applied before and after overload stress levels in the bridge. Evans and Rowlands [8] carried out experimental and theoretical investigations of the behavior of single-cell, single-span box girders on skew supports. The behavior of bridge was analyzed by the FEM. The effect of the skew angle on the behavior of bridge was discussed. Meng et al. [9] described an analytical and experimental study of a skewed bridge model. The FE analyses (FEA) were performed using the commercial software SAP2000. Good agreement between the experimental and FEA results is obtained. Meng and Liu [10] proposed a refined stick model for the preliminary dynamic analysis of skew bridges as well. Badwan and Liang [11] presented an in-site static load test and a FEA on an existing 60° skew, three-span continuous steel girder bridge. The measured bridge response under the test load was used to develop and calibrate a FEM model by using ANSYS software. The calibrated FEM model was demonstrated that it is realistic to predict the bridge response. Menassa et al. [12] reported that the effect of a skew angle on simple-span reinforced concrete bridges using FEM. The commercial FE software SAP2000 was used to generate the three-dimensional finite element models. The results show that the AASHTO Standard Specifications procedure overestimated the maximum longitudinal bending moment when a skew angle is larger than 20°. Since conventional grillage methods

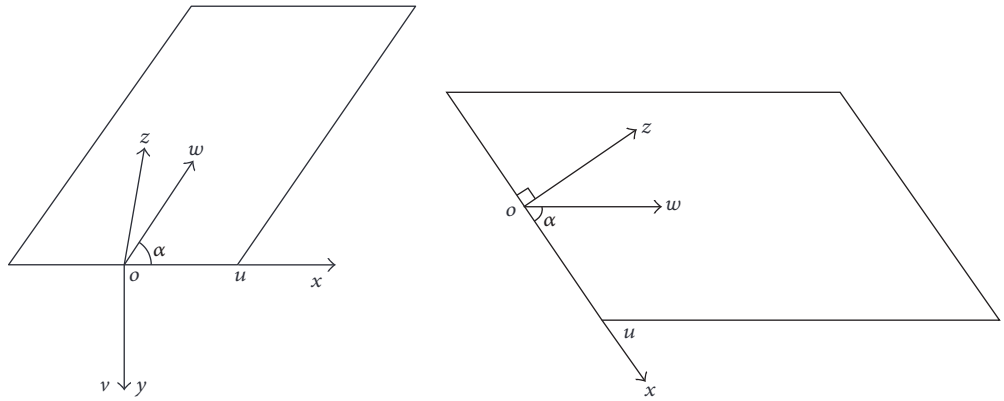

(a) Isometric view (b) Top view

Figure 1: Inclined coordinate system for the top and bottom plates.

cannot account for some important structural actions of thin-walled box girders, the Canadian Highway Bridge Design Code (CHBDC) [13] as well as the American Association of State Highway Transportation Officials (AASHTO) [14, 15] has prohibited the use of the conventional grillage method in the case of certain types of box girder bridges. Due to a large number of degrees of freedom needed, a detailed three-dimensional FEA of box girders performed using commercial FE programs is too complex and time-consuming. Therefore, it is important to develop a practical FEM to reduce the amount of computational work for the analysis of the skewed box girder bridges. Finite segment method has been used to simplify a three-dimensional thin-walled box girder into a one-dimensional structure for curved box girder analysis [16]. But until now, such method used for skew box girder analysis do not appear to be reported in the open literature.

In this study, by modeling the top and bottom plates of a skew box girder with skewed plate beam element and the webs with normal plate beam element, a spatial displacement field for a skewed box girder is constructed. The displacement compatibilities of the subelements at corners are met accordingly. Skewed plate beam element represents that the element is formulated under an inclined coordinate system while the normal plate beam element represents that the element is formulated under an orthogonal coordinate system. The skewed box girder is discretized into finite segments which were assembled by 4-plate beam subelements along the length of the girder. To verify the accuracy of the proposed finite segment method (FSM), the results obtained using this approach were compared with the results obtained by using ANSYS and the tested results from a modal test.

2. Basic Formulae under Inclined Coordinate System

There is an inclined angle between the central line and the support line of the bridge. Therefore, an inclined coordinate system is chosen for the top and bottom plates of the skewed box girder, as shown in Figure 1.

The inclined angle of the specific plates is α; the relationships between the rectangular coordinates ($oxyz$) and the inclined coordinates ($ouvw$) are

$$\begin{aligned} x &= u + w\cos\alpha, \\ y &= v, \\ z &= w\sin\alpha, \\ u &= x - zctg\alpha, \\ v &= y, \\ w &= \frac{z}{\sin\alpha}, \end{aligned} \tag{1}$$

where u, v, and w are the transverse (along the x direction), vertical (along the y direction), and longitudinal displacement (in the z direction) of the top or bottom plate, respectively. Using the derivative principle of the multivariable functions, there is

$$\begin{aligned} \frac{\partial w}{\partial z} &= -\frac{\partial w}{\partial \overline{u}} ctg\alpha + \frac{1}{\sin\alpha}\frac{\partial w}{\partial \overline{w}}, \\ \frac{\partial w}{\partial x} &= \frac{\partial w}{\partial \overline{u}}, \\ \frac{\partial w}{\partial y} &= \frac{\partial w}{\partial \overline{v}}, \\ \frac{\partial v}{\partial z} &= -\cot\alpha\frac{\partial v}{\partial \overline{u}} + \frac{1}{\sin\alpha}\frac{\partial v}{\partial \overline{w}}, \\ \frac{\partial u}{\partial z} &= -\cot\alpha\frac{\partial u}{\partial \overline{u}} + \frac{1}{\sin\alpha}\frac{\partial u}{\partial \overline{w}}, \\ \frac{\partial^2 v}{\partial z^2} &= \cot^2\alpha\frac{\partial^2 v}{\partial \overline{u}^2} - \frac{2\cot\alpha}{\sin\alpha}\frac{\partial^2 v}{\partial \overline{u}\partial \overline{w}} + \frac{1}{\sin^2\alpha}\frac{\partial^2 v}{\partial \overline{w}^2}, \\ \frac{\partial^2 u}{\partial z^2} &= \cot^2\alpha\frac{\partial^2 u}{\partial \overline{u}^2} - \frac{2\cot\alpha}{\sin\alpha}\frac{\partial^2 u}{\partial \overline{u}\partial \overline{w}} + \frac{1}{\sin^2\alpha}\frac{\partial^2 u}{\partial \overline{w}^2}. \end{aligned} \tag{2}$$

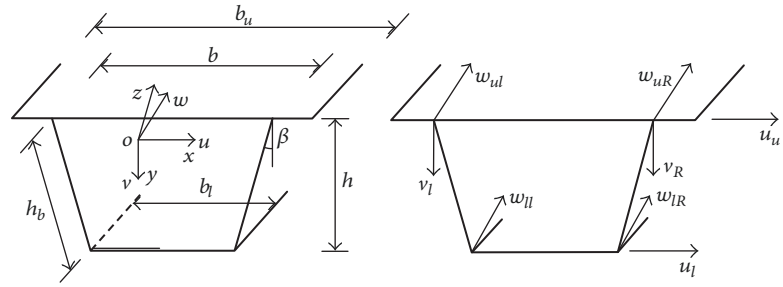

Figure 2: The cross-sectional displacement parameters of a single-cell skewed box girder.

3. Displacement Model of the Cross Section

For convenience of illustration, a single-cell skewed box girder is used as an example herein. The cross-sectional displacement parameters of a single-cell skewed box girder are shown in Figure 2. To establish the displacement model of the spatial skewed box girder, two assumptions based on Vlasov's thin-walled beam theory [17] are adopted in this paper.

(1) As the skewed box girder is discretized into several skewed box girder segments along the length of bridge, the displacement compatibilities of these elements at the locations of corners are satisfied.

(2) The tensile and compressive deformations along the width and height directions of the four walls of the girder are ignored.

For each segment of the single-cell skewed box girder, the section displacement parameters include four longitudinal displacement parameters w_{ul}, w_{uR}, w_{ll}, w_{lR} for the four corners; two transverse displacement parameters u_u and u_l for the top and bottom plates; and two vertical displacement parameters v_l and v_R for the left and right upper corners of the skewed box girder. Hence, there are eight independent displacement parameters for the cross section of the single-cell skewed box girder, that is, w_{ul}, w_{uR}, w_{ll}, w_{lR}, u_u, u_l, v_l, and v_R. The cross-sectional parameters of the skewed box girder segment are all defined in the rectangular coordinates ($oxyz$); that is, the longitudinal displacements of the segment w_{ul}, w_{uR}, w_{ll}, and w_{lR} are along the axial z direction, not along the skewed bridge axial line.

4. Subelement Displacement Parameters

If the whole skewed beam segment of the skewed box girder is taken as one-beam element, the segment can be discretized into wall subelements, by which a suitable subelement displacement mode can be established. According to the thin-walled beam theory [17], the displacement at the gravity center of the subelement cross section is equal to the average value of displacements at the corresponding two nodes and the subelement displacement parameters are determined by the displacements at the two nodes.

The nodal displacement parameters are shown in Figure 3. The subelement displacement parameters are given as follows.

For the left web, we have the following.

The transverse displacement (in the web plane) is

$$u_{fl} = [N(w)]\left\{\delta u_{fl}^*\right\}. \tag{3a}$$

The vertical displacement (out of the web plane) is

$$v_{fl} = [N(w)]\left\{\delta v_{fl}^*\right\}. \tag{3b}$$

The longitudinal displacement (in the $\overline{w}$ direction) is

$$w_{fl} = [M(w)]\left\{\delta w_{fl}^*\right\}. \tag{3c}$$

The torsional angle around axial w is

$$\varphi_{fl} = [M(w)]\left\{\delta \varphi_{fl}^*\right\}. \tag{3d}$$

For the right web, we have the following.

The transverse displacement (in the web plane) is

$$u_{fR} = [N(w)]\left\{\delta u_{fR}^*\right\}. \tag{4a}$$

The vertical displacement (out of the web plane) is

$$v_{fR} = [N(w)]\left\{\delta v_{fR}^*\right\}. \tag{4b}$$

The longitudinal displacement (in the w direction) is

$$w_{fR} = [M(w)]\left\{\delta w_{fR}^*\right\}. \tag{4c}$$

The torsional angle around axial w is

$$\varphi_{fR} = [M(w)]\left\{\delta \varphi_{fR}^*\right\}. \tag{4d}$$

In these above equations, $[N(w)]$ and $[M(w)]$ are cubic shape function matrix and linear shape function matrix about w, respectively. The detailed expressions are as follows:

$$[N(w)] = \begin{bmatrix} N_1(w) & N_2(w) & N_3(w) & N_4(w) \end{bmatrix}, \tag{5a}$$

$$[M(w)] = \begin{bmatrix} M_1(w) & M_2(w) \end{bmatrix}, \tag{5b}$$

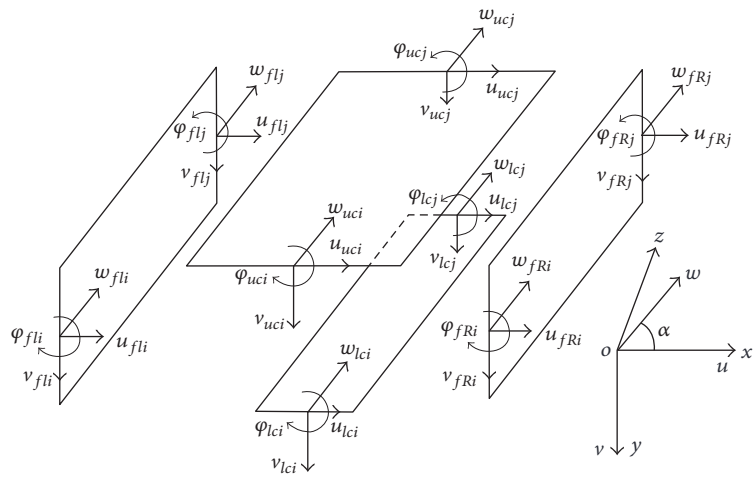

Figure 3: The nodal displacement parameters of the beam subelements.

where

$$N_1(w) = 1 - 3\left(\frac{w}{l}\right)^2 + 2\left(\frac{w}{l}\right)^3,$$

$$N_2(w) = w\left[1 - 2\frac{w}{l} + \left(\frac{w}{l}\right)^2\right],$$

$$N_3(w) = \left(\frac{w}{l}\right)^2\left[3 - 2\frac{w}{l}\right],$$

$$N_4(w) = w\left[-\frac{w}{l} + \left(\frac{w}{l}\right)^2\right],$$

$$M_1(w) = 1 - \frac{w}{l},$$

$$M_2(w) = \frac{w}{l},$$

$$\begin{aligned}
\left\{\delta u^*_{fl}\right\} &= \left[u_{fli} \;\; u'_{fli} \;\; u_{flj} \;\; u'_{flj}\right]^T,\\
\left\{\delta v^*_{fl}\right\} &= \left[v_{fli} \;\; v'_{fli} \;\; v_{flj} \;\; v'_{flj}\right]^T,\\
\left\{\delta w^*_{fl}\right\} &= \left[w_{fli} \;\; w_{flj}\right]^T,\\
\left\{\delta \varphi^*_{fl}\right\} &= \left[\varphi_{fli} \;\; \varphi_{flj}\right]^T,\\
\left\{\delta u^*_{fR}\right\} &= \left[u_{fRi} \;\; u'_{fRi} \;\; u_{fRj} \;\; u'_{fRj}\right]^T,\\
\left\{\delta v^*_{fR}\right\} &= \left[v_{fRi} \;\; v'_{fRi} \;\; v_{fRj} \;\; v'_{fRj}\right]^T,\\
\left\{\delta w^*_{fR}\right\} &= \left[w_{fRi} \;\; w_{fRj}\right]^T,\\
\left\{\delta \varphi^*_{fR}\right\} &= \left[\varphi_{fRi} \;\; \varphi_{fRj}\right]^T.
\end{aligned} \tag{6}$$

For the top and bottom subelements, because of their skew geometry, their displacement parameters are all defined relative to the rectangular coordinate ($oxyz$) for convenience in expressing the stiffness matrices of the specific subelements. Hence, the four nodal transverse displacements u_{uci}, u_{ucj}, u_{lci}, u_{lcj} are along the x direction, the nodal vertical displacements v_{uci}, v_{ucj}, v_{lci}, v_{lcj} are along the y direction, and the longitudinal node displacements w_{uci}, w_{ucj}, w_{lci}, w_{lcj} are along the z direction as shown in Figure 3. The subelement displacement parameters are given as follows:

For the top plate, we have the following.

The transverse displacement (in the x direction) is

$$u_{uc} = [N(w)]\left\{\delta u^*_{uc}\right\}. \tag{7a}$$

The vertical displacement (in the y direction) is

$$v_{uc} = [N(w)]\left\{\delta v^*_{uc}\right\}. \tag{7b}$$

The longitudinal displacement (in the z direction) is

$$w_{uc} = [M(w)]\left\{\delta w^*_{uc}\right\}. \tag{7c}$$

The torsional angle around axial z is

$$\varphi_{uc} = [M(w)]\left\{\delta \varphi^*_{uc}\right\}. \tag{7d}$$

For the bottom plate, we have the following.

The transverse displacement (in the x direction) is

$$u_{lc} = [N(w)]\left\{\delta u^*_{lc}\right\}. \tag{8a}$$

The vertical displacement (in the y direction) is

$$v_{lc} = [N(w)]\left\{\delta v^*_{lc}\right\}. \tag{8b}$$

The longitudinal displacement (in the z direction) is

$$w_{lc} = [M(w)]\left\{\delta w^*_{lc}\right\}. \tag{8c}$$

The torsional angle around axial z is

$$\varphi_{lc} = [M(w)]\left\{\delta \varphi^*_{lc}\right\}, \tag{8d}$$

where

$$\begin{aligned}
\{\delta u_{uc}^*\} &= \left[u_{uci} \;\; u'_{uci} \;\; u_{ucj} \;\; u'_{ucj}\right]^T,\\
\{\delta v_{uc}^*\} &= \left[v_{uci} \;\; v'_{uci} \;\; v_{ucj} \;\; v'_{ucj}\right]^T,\\
\{\delta w_{uc}^*\} &= \left[w_{uci} \;\; w_{ucj}\right]^T,\\
\{\delta \varphi_{uc}^*\} &= \left[\varphi_{uci} \;\; \varphi_{ucj}\right]^T,\\
\{\delta u_{lc}^*\} &= \left[u_{lci} \;\; u'_{lci} \;\; u_{lcj} \;\; u'_{lcj}\right]^T,\\
\{\delta v_{lc}^*\} &= \left[v_{lci} \;\; v'_{lci} \;\; v_{lcj} \;\; v'_{lcj}\right]^T,\\
\{\delta w_{lc}^*\} &= \left[w_{lci} \;\; w_{lcj}\right]^T,\\
\{\delta \varphi_{lc}^*\} &= \left[\varphi_{lci} \;\; \varphi_{lcj}\right]^T.
\end{aligned} \tag{9}$$

5. Relationship between the Displacement Parameters of Subelement and the Section

According to the deformation compatibility condition between the part and the whole, the four walls of the skewed box girder considered as subelement beams are connected at the corners [16].

For the top plate, there are

$$\begin{aligned}
u_{uc} &= u_u,\\
u'_{uc} &= \frac{1}{b}\left(w_{ul} - w_{uR}\right),\\
v_{uc} &= \frac{1}{2}\left(v_l + v_R\right),\\
v'_{uc} &= \frac{1}{2}\left(v'_l + v'_R\right),\\
w_{uc} &= \frac{1}{2}\left(w_{ul} + w_{uR}\right),\\
\varphi_{uc} &= \frac{1}{b}\left(v_R - v_l\right).
\end{aligned} \tag{10}$$

For the bottom plate, there are

$$\begin{aligned}
u_{lc} &= u_l,\\
u'_{lc} &= \frac{1}{b_l}\left(w_{ll} - w_{lR}\right),\\
v_{lc} &= \frac{1}{2}\left(v_l + v_R\right),\\
v'_{lc} &= \frac{1}{2}\left(v'_l + v'_R\right),\\
w_{lc} &= \frac{1}{2}\left(w_{ll} + w_{lR}\right),\\
\varphi_{lc} &= \frac{1}{b_l}\left[v_R - v_l + 2\left(u_l - u_u\right) tg\beta\right].
\end{aligned} \tag{11}$$

Sectional geometry and displacement parameters of the left and right webs of the subelement are shown in Figure 4, where section $A'B'C'D'$ is normal to the center line of the skewed box girder. In view of sectional geometry of skewed box girder and the basic assumptions of the box girder, there are

$$\begin{aligned}
v_{fl}^{\alpha} &= \frac{1}{2}\left[\left(u_c + u_l\right)\sin\alpha - \left(w_{ul} + w_{ll}\right)\cos\alpha\right],\\
v_{fl}^{\alpha} &= \frac{1}{2}\left[2v_l + \left(u_u - u_l\right) tg\beta\right],\\
u_{fl}^{\alpha} &= v_l\cos\beta_1 + \left(u_u\sin\alpha - w_{ul}\cos\alpha\right)\sin\beta_1,\\
w_{fl}^{\alpha} &= \frac{1}{2}\left[\left(u_l + u_u\right)\cos\alpha + \left(w_{ul} + w_{ll}\right)\sin\alpha\right].
\end{aligned} \tag{12}$$

According to the geometric relationship in Figure 4, we obtained

$$\begin{aligned}
u_{fl} &= u_{fl}^{\alpha},\\
w_{fl} &= w_{fl}^{\alpha},\\
v_{fl} &= v_{fl}^{\alpha}\cos\beta_1 + v_l^{\alpha}\sin\beta_1.
\end{aligned} \tag{13}$$

Rearranging (12) and (13) gives the following.
For the left web,

$$\begin{aligned}
u_{fl} &= v_l\cos\beta_1 + \left(u_u\sin\alpha - w_{ul}\cos\alpha\right)\sin\beta_1,\\
u'_{fl} &= \frac{1}{h_b}\left(\left(u_u - u_l\right)\cos\alpha + \left(w_{ul} - w_{ll}\right)\sin\alpha\right),\\
v_{fl} &= \frac{1}{2}\cos\beta_1\left(\left(u_u + u_l\right)\sin\alpha - \left(w_{ul} + w_{ll}\right)\cos\alpha\right)\\
&\quad - \frac{1}{2}\sin\beta_1\left(2v_l + \left(u_u - u_l\right) tg\beta\right),\\
v'_{fl} &= \left(\frac{\cos\beta + tg\beta\sin\beta}{2b_l} + \frac{\sin\beta}{h}\right)\\
&\quad \cdot \left(u_l\cos\alpha + w_{ll}\sin\alpha\right) - \left(\frac{\cos\beta + tg\beta\sin\beta}{2b_l}\right)\\
&\quad \times \left(u_l\cos\alpha + w_{lR}\sin\alpha\right)\\
&\quad + \left(\frac{\cos\beta + tg\beta\sin\beta}{2b} - \frac{\sin\beta}{h}\right)\\
&\quad \cdot \left(u_u\cos\alpha + w_{ul}\sin\alpha\right) - \left(\frac{\cos\beta + tg\beta\sin\beta}{2b}\right)\\
&\quad \cdot \left(u_u\cos\alpha + w_{uR}\sin\alpha\right),\\
w_{fl} &= \frac{1}{2}\left(\left(u_l + u_u\right)\cos a + \left(w_{ll} + w_{ul}\right)\sin\alpha\right),\\
\varphi_{fl} &= \frac{1}{h}\left(u_u\sin\alpha - w_{ul}\cos\alpha - u_l\sin\alpha + w_{ll}\cos\alpha\right).
\end{aligned} \tag{14}$$

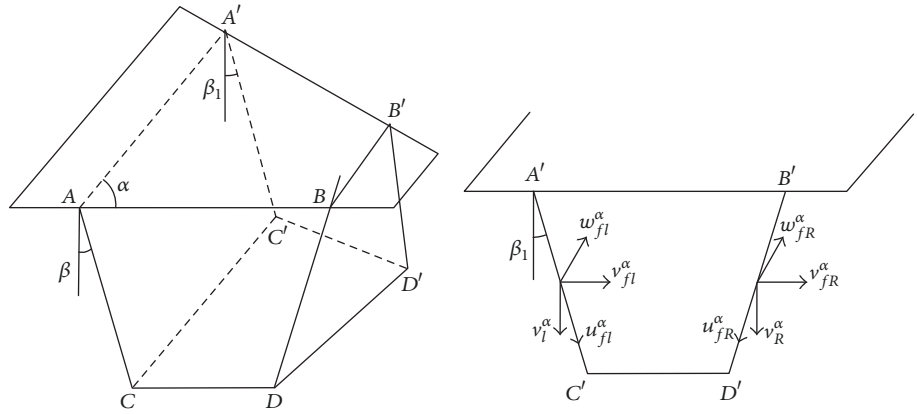

Figure 4: Sectional geometry and displacement parameters of the webs.

For the right web,

$$
\begin{aligned}
u_{fR} &= v_R \cos\beta_1 - (u_u \sin\alpha - w_{uR}\cos\alpha)\sin\beta_1,\\
u'_{fR} &= \frac{1}{h_b}\left((u_u - u_l)\cos\alpha + (w_{uR} - w_{lR})\sin\alpha\right),\\
v_{fR} &= \frac{1}{2}\sin\beta_1\left(2v_R + (u_l - u_u)\,tg\beta\right) + \frac{1}{2}\cos\beta_1\\
&\quad\times\left((u_u + u_l)\sin\alpha - (w_{uR} + w_{lR})\cos\alpha\right),\\
v'_{fR} &= \frac{1}{2b\cos\beta}\left(u_u\cos\alpha + w_{ul}\sin\alpha\right)\\
&\quad+\left(\frac{\sin\beta}{h} - \frac{1}{2b\cos\beta}\right)\left(u_u\cos\alpha + w_{uR}\sin\alpha\right)\\
&\quad+\frac{1}{2b_l\cos\beta}\left(u_l\cos\alpha + w_{ll}\sin\alpha\right)\\
&\quad-\left(\frac{1}{2b_l\cos\beta} + \frac{\sin\beta}{h}\right)\left(u_l\cos\alpha + w_{lR}\sin\alpha\right),\\
w_{fR} &= \frac{1}{2}\left((u_l + u_u)\cos a + (w_{lR} + w_{uR})\sin\alpha\right),\\
\varphi_{fR} &= \frac{1}{h}\left(u_u\sin\alpha - w_{uR}\cos\alpha - u_l\sin\alpha + w_{lR}\cos\alpha\right),
\end{aligned}
\tag{15}
$$

where $\beta_1 = \arctan tg(((b - b_l)/2h)\sin\alpha)$.

According to (10)–(15), each subelement's displacement parameter is related to the cross section's displacement parameters as the following matrix form:

$$
\begin{aligned}
\{d_u\} &= A\{d\},\\
\{d_l\} &= B\{d\},\\
\{d_{fl}\} &= C\{d\},\\
\{d_{fR}\} &= D\{d\},
\end{aligned}
\tag{16}
$$

where

$$
\begin{aligned}
\{d_u\} &= \left[w_{uc}\ \ u_{uc}\ \ v_{vc}\ \ \varphi_{uc}\ \ v'_{uc}\ \ u'_{uc}\right]^T,\\
\{d_l\} &= \left[w_{lc}\ \ u_{lc}\ \ v_{lc}\ \ \varphi_{lc}\ \ v'_{lc}\ \ u'_{lc}\right]^T,\\
\{d_{fl}\} &= \left[w_{fl}\ \ u_{fl}\ \ v_{fl}\ \ \varphi_{fl}\ \ v'_{fl}\ \ u'_{fl}\right]^T,\\
\{d_{fR}\} &= \left[w_{fR}\ \ u_{fR}\ \ v_{fR}\ \ \varphi_{fR}\ \ v'_{fR}\ \ u'_{fR}\right]^T,\\
\{d\} &= \left[u_u\ \ u_l\ \ v_l\ \ v_R\ \ w_{ul}\ \ w_{uR}\ \ w_{ll}\ \ w_{lR}\right]^T,
\end{aligned}
\tag{17}
$$

where A, B, C, and D are the coefficient matrices that are obtained from (10)~(15).

6. Elastic Strain Energy of the Subelements

The transformation relationship between the inclined coordinate and the rectangular coordinate as defined in (1) and (2) was used to calculate the stiffness matrices.

Once the displacement model of the subelements is given, the displacements at arbitrary point of the subelement can be determined.

On the top plate, we have the following.

The transverse displacement (in the x direction) is

$$
u^u = [N(\overline{w})]\{\delta u^*_{uc}\} - \overline{v}\,[M(\overline{w})]\{\delta\varphi^*_{uc}\}. \tag{18a}
$$

The vertical displacement (in the y direction) is

$$
v^u = [N(\overline{w})]\{\delta v^*_{uc}\} - \overline{u}\,[M(\overline{w})]\{\delta\varphi^*_{uc}\}. \tag{18b}
$$

The longitudinal displacement (in the z direction) is

$$
\begin{aligned}
w^u &= [M(\overline{w})]\{\delta w^*_{uc}\} - \overline{u}\frac{\partial}{\partial z}\left([N(\overline{w})]\{\delta u^*_{uc}\}\right)\\
&\quad-\overline{v}\frac{\partial}{\partial z}\left([N(\overline{w})]\{\delta v^*_{uc}\}\right).
\end{aligned}
\tag{18c}
$$

On the bottom plate, we have the following.

The transverse displacement (in the x direction) is

$$u^l = [N(\overline{w})]\{\delta u_{lc}^*\} - \overline{v}[M(\overline{w})]\{\delta\varphi_{lc}^*\}. \tag{19a}$$

The vertical displacement (in the y direction) is

$$v^l = [N(\overline{w})]\{\delta v_{lc}^*\} + \overline{u}[M(\overline{w})]\{\delta\varphi_{lc}^*\}. \tag{19b}$$

The longitudinal displacement (in the z direction) is

$$\begin{aligned} w^l = {} & [M(\overline{w})]\{\delta w_{lc}^*\} - \overline{u}\frac{\partial}{\partial z}\left([N(\overline{w})]\{\delta u_{lc}^*\}\right) \\ & - \overline{v}\frac{\partial}{\partial z}\left([N(\overline{w})]\{\delta v_{lc}^*\}\right). \end{aligned} \tag{19c}$$

Based on (1) and (2), the strain-displacement relationship of the top plate can be written as

$$\begin{aligned} \varepsilon_{zz}^u &= \frac{\partial w^u}{\partial z} \\ &= \frac{1}{\sin\alpha}\left[M'(\overline{w})\right]\{\delta w_{uc}^*\} \\ &\quad + \frac{\cos\alpha}{\sin^2\alpha}\left[N'(\overline{w})\right]\{\delta u_{uc}^*\} \\ &\quad - \frac{\overline{u}}{\sin^2\alpha}\left[N''(\overline{w})\right]\{\delta u_{uc}^*\} \\ &\quad - \frac{\overline{v}}{\sin^2\alpha}\left[N''(\overline{w})\right]\{\delta v_{uc}^*\}, \\ \gamma_{xz}^u &= \frac{\partial w^u}{\partial x} + \frac{\partial u^u}{\partial z} = -\frac{\overline{v}}{\sin\alpha}\left[M'(\overline{w})\right]\{\delta\varphi_{uc}^*\}, \\ \gamma_{yz}^u &= \frac{\partial w^u}{\partial y} + \frac{\partial v^u}{\partial z} \\ &= -\cot\alpha[M(\overline{w})]\{\delta\varphi_{uc}^*\} \\ &\quad + \frac{\overline{u}}{\sin\alpha}\left[M'(\overline{w})\right]\{\delta\varphi_{uc}^*\}. \end{aligned} \tag{20}$$

Similarly, the strain-displacement relationship of the bottom plate can be written as

$$\begin{aligned} \varepsilon_{zz}^l &= \frac{\partial w^l}{\partial z} \\ &= \frac{1}{\sin\alpha}\left[M'(\overline{w})\right]\{\delta w_{lc}^*\} + \frac{\cos\alpha}{\sin^2\alpha}\left[N'(\overline{w})\right]\{\delta u_{lc}^*\} \\ &\quad - \frac{\overline{u}}{\sin^2\alpha}\left[N''(\overline{w})\right]\{\delta u_{lc}^*\} \\ &\quad - \frac{\overline{v}}{\sin^2\alpha}\left[N''(\overline{w})\right]\{\delta v_{lc}^*\}, \\ \gamma_{xz}^l &= \frac{\partial w^l}{\partial x} + \frac{\partial u^l}{\partial z} = -\frac{\overline{v}}{\sin\alpha}\left[M'(\overline{w})\right]\{\delta\varphi_{lc}^*\}, \\ \gamma_{yz}^l &= \frac{\partial w^l}{\partial y} + \frac{\partial v^l}{\partial z} \\ &= -\cot\alpha[M(\overline{w})]\{\delta\varphi_{lc}^*\} + \frac{\overline{u}}{\sin\alpha}\left[M'(\overline{w})\right]\{\delta\varphi_{lc}^*\}. \end{aligned} \tag{21}$$

Thus, the elastic strain energy of the top plate is

$$\begin{aligned} \pi_u &= \frac{1}{2}\int_{\Omega_u} E\left(\varepsilon_{zz}^u\right)^2 d\Omega + \frac{1}{2}\int_{\Omega_u} G\left(\gamma_{xz}^u\right)^2 d\Omega \\ &\quad + \frac{1}{2}\int_{\Omega_u} G\left(\gamma_{yz}^u\right)^2 d\Omega \\ &= \frac{1}{2}\left[\{\delta w_{uc}^*\}^T\{\delta u_{uc}^*\}^T\{\delta v_{uc}^*\}^T\{\delta\varphi_{uc}^*\}^T\right]\left[K^T\right] \\ &\quad \times\left[\{\delta w_{uc}^*\}^T\{\delta u_{uc}^*\}^T\{\delta v_{uc}^*\}^T\{\delta\varphi_{uc}^*\}^T\right]^T, \end{aligned} \tag{22}$$

where $[K^T] = [K_{i,j}{}^T]_{4\times 4}$ $(i, j = 1, 2, 3, 4)$ is the subelement's stiffness matrix of the top plate. Substituting (1), (2), (18a), (18b), and (18c) into (22), the stiffness matrix $[K^T]$ can be obtained.

Similarly, the elastic strain energy of the bottom plate can also be obtained. The shape of the webs has no difference in comparison with conventional beam. Therefore, the expression of the elastic strain energy of webs can be written as

$$\begin{aligned} \pi_{fl} &= \frac{1}{2}\left[\{d_{fli}\}^T\{d_{flj}\}^T\left[K_{fl}\right]\left[\{d_{fli}\}^T\{d_{flj}\}^T\right]^T\right], \\ \pi_{fR} &= \frac{1}{2}\left[\{d_{fRi}\}^T\{d_{fRj}\}^T\left[K_{fR}\right]\left[\{d_{fRi}\}^T\{d_{fRj}\}^T\right]^T\right]. \end{aligned} \tag{23}$$

7. Establishment of Segment Equilibrium Equation

The total elastic strain energy of the skewed box girder segment, which consists of those of its subelements, is given as

$$\pi = \pi_u + \pi_l + \pi_{fl} + \pi_{fR} - \{F\}^{eT}\left[\{d_i\}^T\{d_j\}^T\right]^{eT}, \tag{24}$$

where π_u, π_l, π_{fl}, and π_{fR} are the elastic strain energies of the top plate, the bottom plate, the left web, and the right web, respectively, and the last item of the right-hand side is the work done by external force. $\{F\}^{eT}$ is the vector of nodal force; any forces acted not at the corners of the element should be transformed to the corners according to the shape functions [18].

Rearranging $\left[\{\delta w_{uc}^*\}^T\ \{\delta u_{uc}^*\}^T\ \{\delta v_{uc}^*\}^T\ \{\delta\varphi_{uc}^*\}^T\right]$ into $\left[\{\delta_{ui}\}^T\ \{d_{uj}\}^T\right]$ and $\left[\{\delta w_{uc}^*\}^T\ \{\delta u_{uc}^*\}^T\ \{\delta v_{uc}^*\}^T\ \{\delta\varphi_{uc}^*\}^T\right]^T$ into $\left[\{d_{ui}\}^T\ \{d_{uj}\}^T\right]^T$ gives the elastic strain energy of the top and bottom plates as

$$\begin{aligned} \pi_u = {} & \frac{1}{2}\left[\{\delta w_{uc}^*\}^T\ \{\delta u_{uc}^*\}^T\ \{\delta v_{uc}^*\}^T\ \{\delta\varphi_{uc}^*\}^T\right]\times[K_u] \\ & \times\left[\{\delta w_{uc}^*\}^T\ \{\delta u_{uc}^*\}^T\ \{\delta v_{uc}^*\}^T\ \{\delta\varphi_{uc}^*\}^T\right]^T \end{aligned}$$

$$
\begin{aligned}
&= \frac{1}{2}\left[\{d_{ui}\}^T \ \{d_{uj}\}^T\right] \times [K_u] \\
&\quad \times \left[\{d_{ui}\}^T \ \{d_{uj}\}^T\right]^T, \\
\pi_l &= \frac{1}{2}\left[\{\delta w_{ul}^*\}^T \ \{\delta u_{ul}^*\}^T \ \{\delta v_{ul}^*\}^T \ \{\delta \varphi_{ul}^*\}^T\right] \times [K_l] \\
&\quad \times \left[\{\delta w_{ul}^*\}^T \ \{\delta u_{ul}^*\}^T \ \{\delta v_{ul}^*\}^T \ \{\delta \varphi_{ul}^*\}^T\right]^T \\
&= \frac{1}{2}\left[\{d_{li}\}^T \ \{d_{lj}\}^T\right] \times [K_l] \times \left[\{d_{li}\}^T \ \{d_{lj}\}^T\right]^T.
\end{aligned} \tag{25}
$$

Substituting (23), (25) into (24) gives

$$
\begin{aligned}
\pi = &\frac{1}{2}\left[\{d_{ui}\}^T \ \{d_{uj}\}^T\right][K_u]\left[\{d_{ui}\}^T \ \{d_{uj}\}^T\right]^T + \frac{1}{2} \\
&\cdot \left[\{d_{li}\}^T \ \{d_{lj}\}^T\right][K_l]\left[\{d_{li}\}^T \ \{d_{lj}\}^T\right]^T + \frac{1}{2} \\
&\cdot \left[\{d_{fli}\}^T \ \{d_{flj}\}^T\right][K_{fl}]\left[\{d_{fli}\}^T \ \{d_{flj}\}^T\right]^T \\
&+ \frac{1}{2}\left[\{d_{fRi}\}^T \ \{d_{fRj}\}^T\right][K_{fR}] \\
&\cdot \left[\{d_{fRi}\}^T \ \{d_{fRj}\}^T\right]^T - \{F\}^{eT}\left[\{d_i\}^T \ \{d_j\}^T\right]^T.
\end{aligned} \tag{26}
$$

Substituting (16) into (26) and applying the variation principle give

$$
\begin{aligned}
&\left(\begin{bmatrix} A & 0 \\ 0 & A \end{bmatrix}^T [K_u] \begin{bmatrix} A & 0 \\ 0 & A \end{bmatrix} + \begin{bmatrix} B & 0 \\ 0 & B \end{bmatrix}^T [K_l] \begin{bmatrix} B & 0 \\ 0 & B \end{bmatrix}\right. \\
&+ \begin{bmatrix} C & 0 \\ 0 & C \end{bmatrix}^T [K_{fl}] \begin{bmatrix} C & 0 \\ 0 & C \end{bmatrix} \\
&\left.+ \begin{bmatrix} D & 0 \\ 0 & D \end{bmatrix}^T [K_{fR}] \begin{bmatrix} D & 0 \\ 0 & D \end{bmatrix}\right) \begin{Bmatrix} \{d_i\} \\ \{d_i\} \end{Bmatrix} = \{F\}^e.
\end{aligned} \tag{27}
$$

We constructed the following equations:

$$
\{\delta\}^e = \left[\{d_i\}^T \ \{d_j\}^T\right]^T, \tag{28a}
$$

$$
\begin{aligned}
[K]^e = &\left(\begin{bmatrix} A & 0 \\ 0 & A \end{bmatrix}^T [K_u] \begin{bmatrix} A & 0 \\ 0 & A \end{bmatrix}\right. \\
&+ \begin{bmatrix} B & 0 \\ 0 & B \end{bmatrix}^T [K_l] \begin{bmatrix} B & 0 \\ 0 & B \end{bmatrix} \\
&+ \begin{bmatrix} C & 0 \\ 0 & C \end{bmatrix}^T [K_{fl}] \begin{bmatrix} C & 0 \\ 0 & C \end{bmatrix} \\
&\left.+ \begin{bmatrix} D & 0 \\ 0 & D \end{bmatrix}^T [K_{fR}] \begin{bmatrix} D & 0 \\ 0 & D \end{bmatrix}\right).
\end{aligned} \tag{28b}
$$

So (27) can rewritten as

$$
[K]^e \{\delta\}^e = \{F\}^e. \tag{29}
$$

This is the equilibrium equation of the segment, where $[K_u]$, $[K_l]$, $[K_{fl}]$, and $[K_{fR}]$ are the subelement's stiffness matrices of the top plate, the bottom plate, the left web, and the right web, respectively. $[K_u]$ and $[K_l]$ can be obtained by rearranging the cross section's displacement parameters into (21). The form of $[K_{fl}]$ and $[K_{fR}]$ is same as that of the stiffness matrix of the conventional spatial beam element. By using the same assembling method as the conventional finite element method, the global stiffness matrices and equilibrium equation can be established and solved.

8. Examples

8.1. Model Bridge Description. A three-span continuous prestressed reinforced concrete skewed box girder bridge was tested by He et al. [1]. The skew angle of the box girder is 45° and the bridge spans are 5.0 + 8.75 + 5.0 m. The widths of the model girder flanges were 1.65 m at the top and 0.85 m at the bottom. The bridge height at mid-span of the main span was 0.375 m and at the piers the height was 0.625 m. The top flange thickness varied between 40 mm and 77 mm, the bottom flange thickness varied between 70 mm and 90 mm, and the web thickness was 100 mm except for the support sections. The evaluation of the bridge modal and typical cross sections are shown in Figure 5. Young's modulus E and Poisson's ratio μ of the girder are 42.54 GPa and 0.3, respectively.

8.2. Loading Description. Two load cases were considered, as shown in Figure 6 and Table 1. The model box girder was instrumented to record displacements and strains during static testing. Instrumentation consisted of 22 displacement transducers, each having 0.01 mm precision, mounted on the two sides of the box girder's webs near the bottom, and more than 100 resistance strain gauges measuring concrete and steel reinforcement strains. Static loads were applied using nine jacks and spreader beams.

8.3. Results and Discussion. The commercial finite element program ANSYS 14.0 was used to validate the accuracy of the proposed finite segment method (FSM). A linear 3D FE model was established. The girder was modeled with 3D block element Solid45, and the FE model is shown in Figure 7. The modal bridge is discretized into 14712 solid elements. For the proposed method, the skewed box girder structure is divided into 10 skewed box girder segments so that each segment of the bridge is subjected to nodal loads only.

The deflection distributions of the webs calculated by the proposed FSM are compared with the experimental results and ANSYS results in Figures 8 and 9. The torsional angle distributions of the section calculated by the proposed FSM and tested results are compared in Figure 10.

From Figures 8 and 9, it can be seen that the results obtained using the proposed finite segment method agree well with that calculated by ANSYS and the tested results which verified the accuracy of the proposed method. For

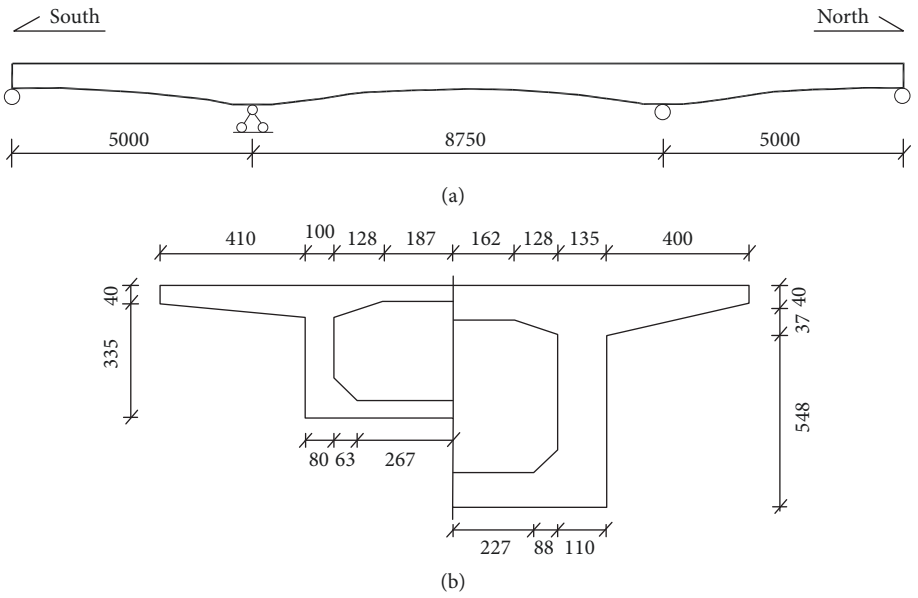

Figure 5: Model bridge (unit: mm). (a) shows elevation, and (b) shows typical cross sections.

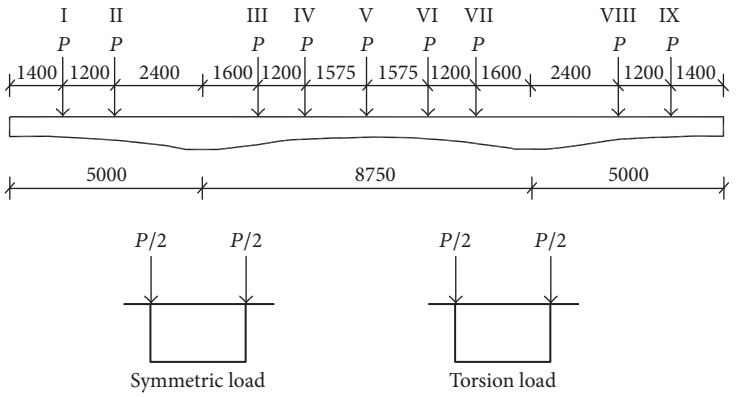

Figure 6: Static loading arrangement.

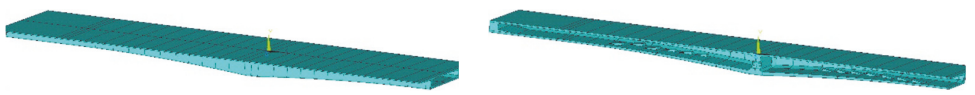

Figure 7: Finite element model. (a) shows the half structure, and (b) is the section of (a).

Table 1: Load cases (unit: kN).

Loading condition	Position at the section	Section								
		I-I	II-II	III-III	IV-IV	V-V	VI-VI	VII-VII	VIII-VIII	IX-IX
Symmetrical	Left	52.5	115	50	65	72.5	65	50	115	52.5
	Right	52.5	115	50	65	72.5	65	50	115	52.5
Torsional	Left	52.5	115	50	65	72.5	40	50	100	20
	Right	20	100	50	40	72.5	65	50	115	52.5

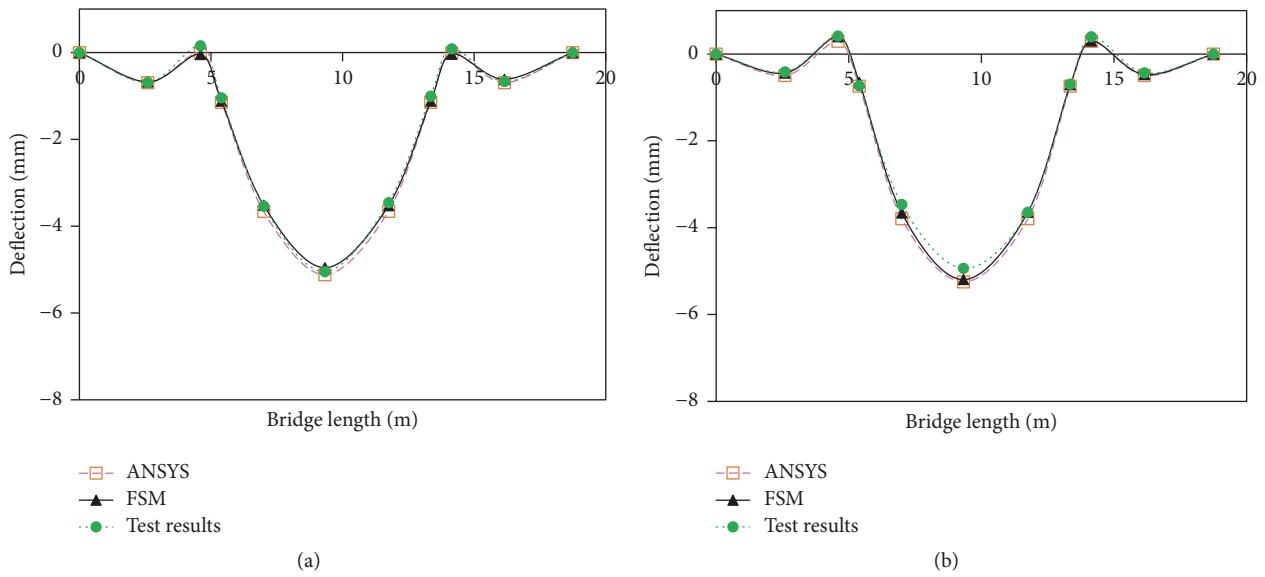

Figure 8: The deflection distribution of the web along the bridge length under symmetric loads. (a) is the left web, and (b) is the right web.

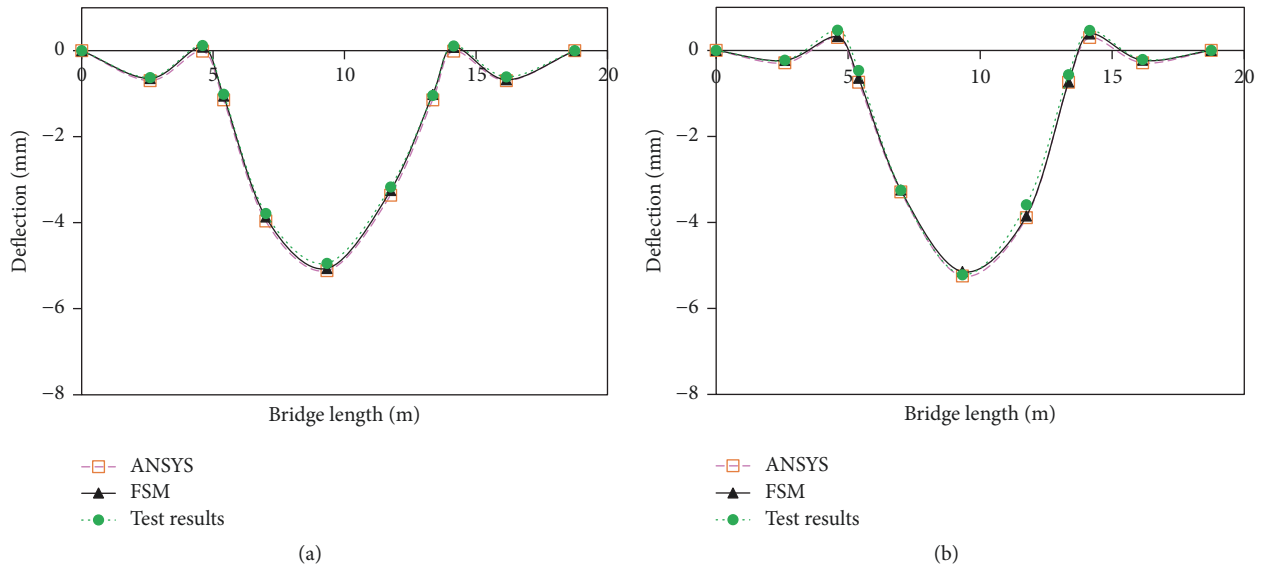

Figure 9: The deflection distribution of the web along the bridge length under torsional loads. (a) is the left web, and (b) is the right web.

symmetric loading, the deflection distribution of the webs along the length of the bridge is symmetrical. And the vertical deflection of the left web is almost the same as that of the right web. For torsional loading, the symmetrical characteristic of the deflection distribution of the web along the length of the bridge is not as good as symmetric loading. For the left web, the deflection of the left part of the main span is larger than that of the right part, while, for the right web, the deflection of the right part of the main span is larger than that of the left part, which are consistent with the characteristics of the load.

The value of deflections and differences between the results of FSM and test in section IV-IV, V-V and VI-VI are listed in Table 2. It can be seen that the results calculated by the proposed method are close to the tested results. For symmetric loading, the maximum differences of the left web and right web between the FSM results and the tested results are no more than 2.1% and 5.4%, respectively. For torsional loading, the maximum differences of the left web and right web between the FSM results and the tested results are no more than 2.5% and 6.1%, respectively.

From Figure 10, it can be seen that the torsional angle distribution along the length of the bridge is basically anti-symmetric for both symmetric loading and torsional loading.

Because the number of the discretized elements in ANSYS model is much larger than the proposed FSM, the computational time of the proposed method is saved largely. In

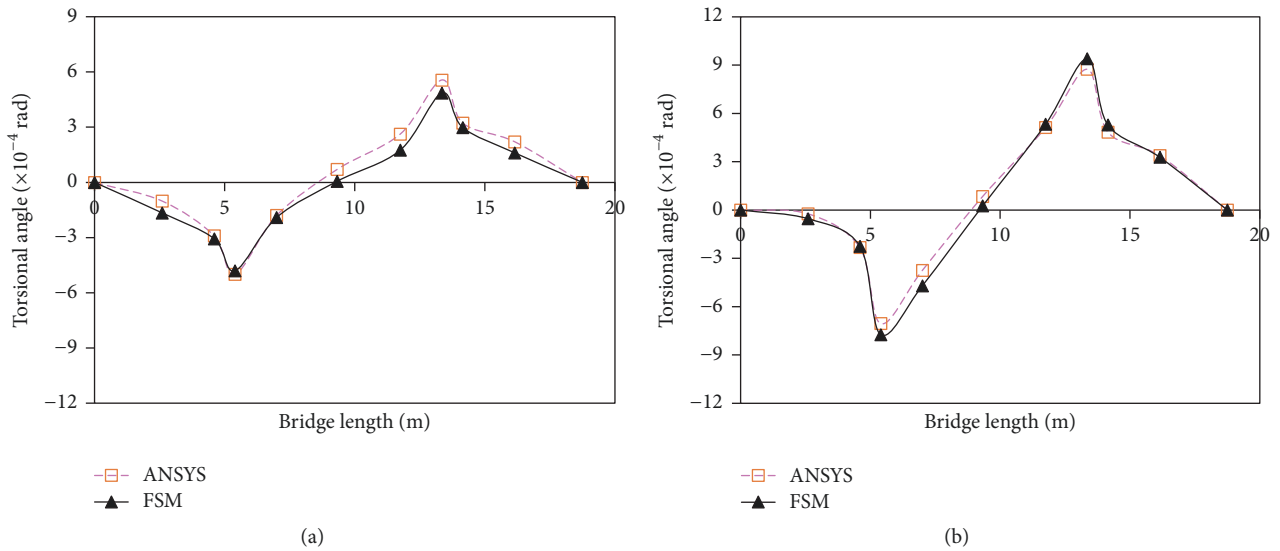

Figure 10: The torsional angle distribution along the bridge length. (a) is the symmetric load, and (b) is the torsional load.

Table 2: Comparisons of deflections (unit: mm).

Load cases	Position	Left web			Right web		
		FSM	Test	Difference	FSM	Test	Difference
Symmetric load	IV	−3.513	−3.539	−0.7%	−3.660	−3.463	5.4%
	V	−4.956	−5.046	−1.8%	−5.196	−4.935	5.0%
	VI	−3.526	−3.454	2.1%	−3.631	−3.646	−0.4%
Torsional load	IV	−3.868	−3.786	2.2%	−3.220	−3.251	−1.0%
	V	−5.064	−4.946	2.4%	−5.145	−5.218	−1.4%
	VI	−3.252	−3.172	2.5%	−3.825	−3.591	6.1%

other words, the proposed FSM is more efficient than the conventional finite element method. In these examples, using the same computer Dell R1308 PC with a four-core Intel i3-3100 2.4 GHz CPU and AMD Radeon HD 4500 graphics card, the solution time of the ANSYS is 436 s while that of the FSM is 2.1 s, from which it can be seen that the computational time is saved significantly.

9. Conclusions

In this paper, a finite segment method was presented to analyze the mechanical behavior of the skewed box bridges. Using the skewed plate beam element under inclined coordinate system for the skewed top and bottom plates and normal plate beam element for the webs, a spatial displacement field for the skewed box girder is constructed. The displacement function is directly constructed according to the behavior of the skewed box girder. The skewed box girder is discretized into finite segments along the length of the girder with each segment assembled by 4 plate beam subelements. The compatibility condition of the displacement at corners of subelements is satisfied accordingly. The stiffness matrix of the finite segment is established based on the potential variation principle and, by using the same assembling method as the conventional finite element method, the global stiffness matrices and equilibrium equation can be established and solved. A model test and the commercial FEM software ANSYS 14.0 were adopted to verify the accuracy of the proposed method. The agreement among the tested results, results obtained by ANSYS, and the proposed finite segment method is good, which demonstrates that the present method is accurate and efficient. Compared with the conventional finite element method, the major advantage of this approach lies in that it can simplify a three-dimensional structure into a one-dimensional structure for analysis and therefore reduces the computational efforts significantly. The proposed method is especially suitable to analyze the global behavior of the skew box girder bridge such as the global stiffness and deflection, and it is a cost-effective method in preliminary design of bridge.

Notations

$\{d\}$: Displacement vector of the beam segment of the skewed box girder
$\{d_{fl}\}$: Displacement vector of the left web
$\{d_{fR}\}$: Displacement vector of the right web

$\{d_l\}$: Displacement vector of the bottom plate
$\{d_u\}$: Displacement vector of the top plate
$[M(w)]$: Linear shape function matrix of the subelement
$[N(w)]$: Cubic shape function matrix of the specified subelement
$\{u_{fl}\}$: Transverse displacement at the center of gravity of the left web
$\{u_{fR}\}$: Transverse displacement at the center of gravity of the right web
$\{u_l\}$: Transverse displacement of the bottom plate for the box girder
$\{u^l\}$: Transverse displacement at an arbitrary point of the subelement of bottom plate
$\{u_{lc}\}$: Transverse displacement at the center of gravity of the bottom plate
$\{u_u\}$: Transverse displacement of the top plate for the box girder
$\{u^u\}$: Transverse displacement at an arbitrary point of the subelement of top plate
$\{u_{uc}\}$: Transverse displacement at the center of gravity of the top plate
$\{v_l\}$: Vertical displacement of the upper-left corner for the box girder
$\{v^l\}$: Vertical displacement at an arbitrary point of the subelement of bottom plate
$\{v_{fl}\}$: Vertical displacement at the center of gravity of the left web
$\{v_{fR}\}$: Vertical displacement at the center of gravity of the right web
$\{v_{lc}\}$: Vertical displacement at the center of gravity of the bottom plate
$\{v_R\}$: Vertical displacement of the upper-right corner for the box girder
$\{v^u\}$: Vertical displacement at an arbitrary point of the subelement of top plate
$\{v_{uc}\}$: Vertical displacement at the center of gravity of the top plate
$\{w_{fl}\}$: Longitudinal displacement at the center of gravity of the left web
$\{w_{fR}\}$: Longitudinal displacement at the center of gravity of the right web
$\{w^l\}$: Longitudinal displacement at an arbitrary point of the subelement of bottom plate
$\{w_{lc}\}$: Longitudinal displacement at the center of gravity of the bottom plate
$\{w_{ll}\}$: Longitudinal displacement for the skewed box girder at lower-left corner
$\{w_{lR}\}$: Longitudinal displacement for the skewed box girder at lower-right corner
$\{w^u\}$: Longitudinal displacement at an arbitrary point of the subelement of top plate
$\{w_{uc}\}$: Longitudinal displacement at the center of gravity of the top plate
$\{w_{ul}\}$: Longitudinal displacement for the skewed box girder at upper-left corner
$\{w_{uR}\}$: Longitudinal displacement for the skewed box girder at upper-right corner
$\{\varphi_{fl}\}$: Rotation angle at the center of gravity of the left web
$\{\varphi_{fR}\}$: Rotation angle at the center of gravity of the right web
$\{\varphi_{lc}\}$: Rotation angle at the center of gravity of the bottom plate
$\{\varphi_{uc}\}$: Rotation angle at the center of gravity of the top plate.

Conflicts of Interest

The authors declare that there are no conflicts of interest regarding the publication of this paper.

Acknowledgments

The authors wish to acknowledge the financial supports from the project of the Basic Research Project for Universities of Liaoning Province (Grant no. LJZ2017043); Postdoctoral Innovation Fund Project of Shenyang Jianzhu University (Grant no. SJZUBSH201712); Liaoning Natural Science Foundation (Grant no. 201602602); Shenyang Science and Technology Fund (Grant no. F16-095-1-00); Ministry of Housing and Urban and Rural Construction Science and Technology Project (Grant no. 2016-K2-012).

References

[1] X. H. He, X. W. Sheng, A. Scanlon, D. G. Linzell, and X. D. Yu, "Skewed concrete box girder bridge static and dynamic testing and analysis," *Engineering Structures*, vol. 39, pp. 38–49, 2012.

[2] S. T. Wasti and A. C. Scordelis, "Comparative structural behavior of straight, curved, and skew reinforced concrete box girder bridge models," in *Proceeding of NATO, Advanced Study Institute on Analysis and Design of Bridges*, pp. 191–211, Izmir, Turkey, 1982.

[3] A. Abdel-Mohti and G. Pekcan, "Seismic response of skewed RC box-girder bridges," *Earthquake Engineering and Engineering Vibration*, vol. 7, no. 4, pp. 415–426, 2008.

[4] B. Zakeri, J. E. Padgett, and G. G. Amiri, "Fragility analysis of skewed single-frame concrete box-girder bridges," *Journal of Performance of Constructed Facilities*, vol. 28, no. 3, pp. 571–582, 2014.

[5] D. B. Ashebo, T. H. T. Chan, and L. Yu, "Evaluation of dynamic loads on a skew box girder continuous bridge part I: field test and modal analysis," *Engineering Structures*, vol. 29, no. 6, pp. 1052–1063, 2007.

[6] B. A. Demeke, H. T. C. Tommy, and Y. Ling, "Evaluation of dynamic loads on a skew box girder continuous bridge Part I: field test and modal analysis," *Engineering Structures*, vol. 29, no. 6, pp. 1064–1073, 2007.

[7] A. C. Scordelis, J. G. Bouwkamp, S. T. Wasti, and F. Seible, "Ultimate strength of skew RC box girder bridge," *Journal of the Structural Division*, vol. 108, no. 1, pp. 105–121, 1982.

[8] H. R. Evans and D. V. Rowlands, "An experimental and theoretical investigation of the behavior of box girders on skew supports," *Civil Engineering for Practicing and Design Engineers*, vol. 4, no. 3, pp. 211–230, 1985.

[9] J. Meng, H. Ghasemi, and E. M. Lui, "Analytical and experimental study of a skew bridge model," *Engineering Structures*, vol. 26, no. 8, pp. 1127–1142, 2004.

[10] J.-Y. Meng and E. M. Lui, "Refined stick model for dynamic analysis of skew highway bridges," *Journal of Bridge Engineering*, vol. 7, no. 3, pp. 184–194, 2002.

[11] I. Z. Badwan and R. Y. Liang, "Reaction distribution in highly skewed continuous steel girder bridge: testing and analysis," *Transportation Research Record*, no. 2028, pp. 163–170, 2007.

[12] C. Menassa, M. Mabsout, K. Tarhini, and G. Frederick, "Influence of skew angle on reinforced concrete slab bridges," *Journal of Bridge Engineering*, vol. 12, no. 2, pp. 205–214, 2007.

[13] CHBDC, *Ontario Ministry of Transportation and Communications*, Canadian Highway Bridge Design Code, Downsview, Ontario, Canada, 2000.

[14] AASHTO, *AASHTO LRFD Bridge Design Specifications*, AASHTO, Washington, Wash, USA, 1994.

[15] AASHTO, *Standard Specifications for Highway Bridges*, AASHTO, Washington, Wash, USA, 1996.

[16] R. H. Wang, Q. S. Li, J. R. Wu, and J. Tang, "A spatial elastic displacement model for curved box girders with corner stiffeners," *Computers Structures*, vol. 83, no. 12-13, pp. 1021–1029, 2005.

[17] V. Z. Vlasov, "Thin-walled elastic beams," Tech. Rep. OTS61-11400, National Science Foundation, Washington, Wash, USA, 1965.

[18] O. C. Zienkiewicz and R. L. Taylor, *The Finite Element Method for Solid and Structural Mechanics*, Butterworth-Heinemann, Oxford, England, 2nd edition, 2000.